Synthesis of Amorphous Al-based Alloy Powders by Mechanical Alloying and Mechanical Disordering

Sci. Rep. RITU A39 (1994) pp. 103-119
No. 2, January 1994

Synthesis of Amorphous Al-based Alloy Powders by Mechanical Alloying and Mechanical Disordering*

M. Sherif EL-ESKANDARANY[1], Kiyoshi AOKI and Kenji SUZUKI
[1]*Mining and Petroleum Engineering Department, Faculty of Engineering, Al-Azhar university, Nasr city, Cairo-Egypt*
Institute for Materials Research, Tohoku University, Sendai 980, Japan

(Received December 28 , 1993)

Amorphous Al-based alloy powders have been synthesized by mechanical alloying (MA) of elemental Al and TM (TM; Ti, Zr, Nb and Ta), and mechanical disordering (MD) from crystalline intermetallic compound powders of Al_xTM_{1-x} respectively using both ball-milling (BM) and rod-milling (RM) techniques. The mechanically alloyed and mechanically disordered alloys were characterized by means of X-ray diffraction, scanning electron microscopy, electron probe microanalysis, transmission electron microscopy, differential thermal analysis, differential scanning calorimetry and chemical analysis.

The results have shown that the crystal-to-amorphous transformation in the MD process occurs through one stage without compositional change, while the crystalline-to-amorphous formation in the MA process occurs through three stages with dramatic compositional change. At the early stage of the MA time, the starting elemental powders of Al and TM are agglomerated to form large composite particles, as large as 800 μm in diameter. These particles contain many thick layers of Al and TM metals. At the intermediate stage of the MA time, however, the powder particles are reduced in size and contain numerous narrow and well-arranged layers. During this stage of MA, a complete crystalline-to-amorphous phase transformation occurs by heating the alloy powders to about 700 K. This transformation occurs due to a thermally assisted solid-state amorphization (TASSA) between the elemental starting materials. Contrary to this, the formation of the amorphous phase at the final stage of the MA time occurs only due to the mechanically driven solid-state amorphization (MDSSA).

KEYWORDS: amorphous alloys, solid state reaction, mechanical alloying, mechanical disordering, powder metallurgy

1. Introduction

The first example of two pure crystalline metals reacting to form a single-phase amorphous alloy was given by Schwarz and Johnson[1]. In this experiment, thin films of pure gold and lanthanum, a few tenths of a nm in thickness, were fully reacted at 343 K within a few ks. Two requirements have been proposed for the solid-state amorphizing reaction: (a) the two reacting metals must have a large negative heat of mixing and (b) the two metals must vastly different diffusivities in each other and in the amorphous alloy to be formed. The first condition ensures that a thermodynamic driving force for the reaction exists. The second condition ensures that the amorphous alloy will form in preference to crystalline intermetallics, which have lower free energies. This kinetic selection of the reaction path is possible because one species diffusing in the other and in the amorphous alloy is sufficient for the solid state amorphizing reaction. The micro-mechanism of the solid-state amorphizing reaction in multilayers was studied by Rutherford back-scattering spectroscopic (RBS) marker experiments on a Ni/Zr diffusion couple[2] and transmission electron microscopy (TEM) on Co/Zr[3]. These experiments showed that the smaller atom in the diffusion couple is the moving species. The growth rate of the amorphous layer, which is formed at the interface of the two atomic species, turned out to be determined by the diffusion coefficient through this amorphous layer.

A different attractive technique for preparation of amorphous materials at temperatures below the crystallization temperature is mechanical alloying (MA) of elemental crystalline powders or the grinding of the crystalline alloy, that is to say, mechanical grinding (MG)[4]. White[5] first reported the amorphization of Nb_3Sn by MA and then Koch et al.[6] established the synthesis of amorphous $Ni_{60}Nb_{40}$ powders by milling a mixture of pure elements. In a typical experiment for preparation of an amorphous $Ni_{60}Nb_{40}$ alloy, elemental powders of Ni and Nb were milled for about 40 ks in He gas using a Spex Mixer/Mill Model 8000 and steel balls as a milling media. The end-product of amorphous $Ni_{60}Nb_{40}$ alloy powders was contaminated with oxygen (0.43 wt.%) and Fe (4.11 wt.%).

The MA process is based on the solid-state amorphizing reaction. It is worth noting that the composition range for which amorphous metallic alloys produced by MA is larger than that for melt quenching, where the glass-forming concentrations are centered around the eutectic composition. One significant potential technological attraction of MA process is that the resulting amorphous powders may subsequently be consolidated by hot pressing at temperatures below the crystallization temperature of the amorphous alloy, thereby offering the prospect of manufacture of bulk objects made from amorphous metallic alloys, without loss of their unique physical properties, a circumstance which is impossible using melt-quenching techniques[7].

In fact, the MA process dates back to 1970 when Benjamin[8] employed the ball-milling technique (BM) for producing homogeneous composite particles with intimately dispersed, uniform internal structure. So far, the

*IMR, Report No.1954

MA process has been used for preparing many dispersion-strengthened alloy powders[9-15].

Comparable to MA process, amorphous alloys can be prepared by MG. Yermakov et al.[4] first reported that the mechanical attrition of crystalline intermetallic compounds of Y and Co led to the formation of an amorphous alloy powder. The MA process synthesizes amorphous alloys by reacting elemental crystalline powders, being accompanied with negative heat of formation. In MG process, however, crystalline alloy or compound powders are transformed into amorphous solid powders by destroying the periodical long-range order of atomic arrangement without compositional changes[16]. MA and MG processes are the reactions going to thermodynamically opposite each other[17].

In MA, the powders are severely deformed, fractured and mutually cold welded during collisions of the balls. Conditions during the violent collisions of grains and balls are not isothermal[18]. The successive deformation and welding of grains leads to a progressively refined lamellar type of domain structure when two elemental metal powders are mechanically alloyed as was shown by Hellstern and Schulz[19]. Schwarz et al.[20] argues that the process of amorphization by MA process leads to an ultrafine composite in which a solid-state amorphizing reaction takes place. This is much the same explanation offered by Atzmon for amorphization of Cu-Er composites at ambient temperature by near isothermal cold rolling [21].

The MA process via BM technique has been considered as a practical solution for amorphizing the systems which are difficult or impossible to be obtained by conventional melting and/or casting techniques, e.g. Al-Ta[22], Al-Nb[23-25] and Cu-Ta[26] binary systems. Moreover, it has been used for preparing amorphous silicon powders by milling elemental silicon powders under purified argon gas in a ball mill[27].

More recently, El-Eskandarany et al.[28-29] have reported the first novel technique for the formation of metal nitride by milling elemental TM (TM; Ti and Fe) powders under flow of nitrogen at room temperature using the reactive ball milling (RBM) process. The RBM leads to the formation of high stable amorphous AlTa contains 15 at.% of nitrogen[30]. Within the last few years a lot of research activity has concentrated on the formation of amorphous and/or compounds alloy powders by BM process[31-66].

In 1990, El-Eskandarany et al.[67] reported another novel technique for producing amorphous $Al_{30}Ta_{70}$ alloy powders from pure aluminium and tantalum powders by a method called rod-milling. This unique technique has been accepted as a successful method for producing amorphous alloy powders with low degree of contamination, that is to say, iron contamination and high thermal stability through solid-state amorphizing reaction[68]. The application of this new technique has led to the formation of many amorphous alloy powders[69-73].

In 1988, Weeber and Bakker[74] reviewed the experimental evidence for amorphization by MA and MG methods. More recently, Suzuki[75] and Koch[76] have reported another review papers about the amorphization reaction via the BM technique.

The present study has been addressed in part to the investigating the morphology, structure and thermodynamic behaviors of amorphous Al-TM alloy powders produced by RM technique. Such systems are of interest for several reasons:

First, they have good thermal properties, such as high thermal stability which make them as a high rank alloys for several industrial applications[77]. Moreover, these alloys specially Al-Ta binary system is difficult or impossible to be produced by conventional melting and casting techniques due to the great difference of the melting points between metallic Al (933 K) and Ta (3293 K), as shown in Fig.1 which presents the equilibrium phase diagram of Al-Ta binary system[78]. Therefore, MA process allows the fabrication of such a new amorphous alloy with a wide range of formation.

Secondly, systematic and comparative study of the amorphization process via different milling techniques (balls and/or rods) and different processes (MA and/or MG).

The last aim was to make a systematic study of a

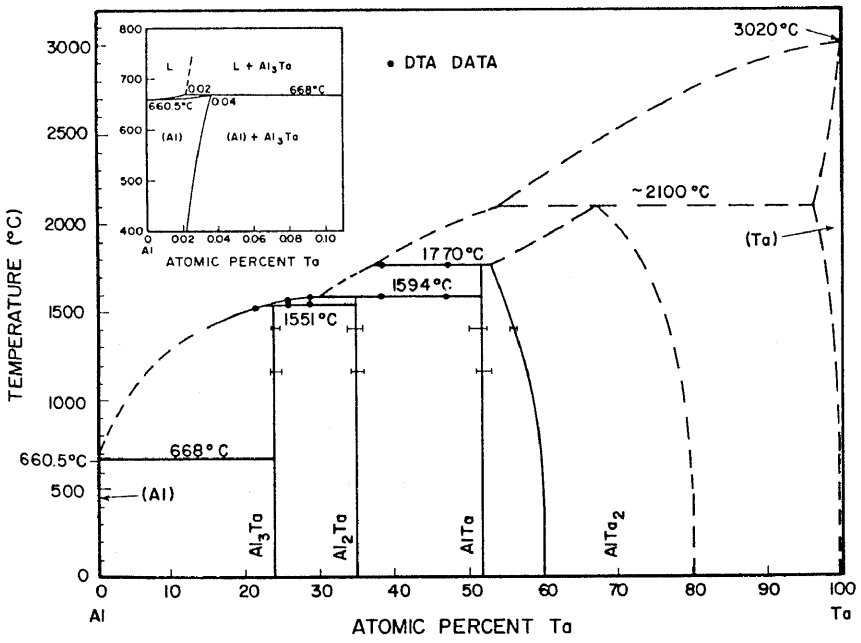

Fig. 1 Phase relation of Al-Ta binary system (ref. 78).

group of systems for which there are no or very few thermodynamic data.

2. Experimental

2.1. Materials

In the present work, a high purity (99.99 %) elemental powders of Al and TM (TM; Ti, Zr, Nb and Ta) metals have been used for the mechanical alloying (MA) experiments. The average particle size of Al and TM elements was 40 and 80 μm, respectively. The metal powders were sealed under high purified argon gas (O_2 and H_2O were less than 1 ppm). In the mechanical disordering (MD) experiments, however, high purity (99.999 %, 3 mm thickness) metal plates of Al and TM were used for preparing intermetallic compounds.

2.2. Types of Mill

The tumbling mills used in this study are cylindrical in shape and rotate about a horizontal axis. A load of milling bodies (balls or rods) is called the milling media which forms a part of the milling load. In these mills, the powder particles of two metals in the tumbling mixture meets the impacting, abrasive and/or shear forces which causes a solid-state diffusion of the two metals powder. Ball mills and rod mills fall under this category.

2.2.1.1. Ball mill

Stainless steel (SUS 304) vial (108 mm inner diameter x 105 mm in length) containing 25 stainless steel balls (SUS 304, 14 and 19 mm in diameter) used as the milling tool. The ball-mill which used in the present study was described in details elsewhere[79].

2.2.1.2. Rod mill

The rod mill has been designed so that its length (250 mm) is greater than its diameter (120 mm) and the rods (SUS 304, 10 mm in diameter) have been cut to lengths (200 mm) less than the full length of the shell. The movement of the rods (10 rods) inside the shell was directly observed through a thick and transparent plastic plate sealing the window of the shell. This observation has shown that the milling process occurs by the line contact of rod-powders-rod extending over the full length of the shell. More details of the rod-mill can be found in a previous paper[67]. In the present work, the ball milling and/or rod milling were carried out by mounting the shells on a rotator running at a rate of 1.4 s^{-1}.

2.3. Sample Preparation

The starting materials of the MA or MD process were placed in a glove box, together with the milling tools. The glove box was evacuated for 3.6 ks by a rotary pump. Then, a purified argon gas (O_2 and H_2O were less than 1 ppm) was flushed into the glove box. In order to minimize the O_2 contamination content, the glove box was evacuated at least two times. In the MA experiments, the elemental powders of Al and TM metals were blended using a ceramics mortar and pestle in the glove box to give the desired composition of Al_xTM_{1-x} binary systems. The blended powders were sealed in the mill together with the milling media. We have used 1200 g of the milling media and about 35 g of the powders to give a weight ratio as 36:1. On the other hand, the starting material for the MD process was prepared by arc-melting nominal amounts of Al and Ta plates in an argon atmosphere purified with a Ti getter. To insure homogeneity, the ingot was remelted five times, reweighed and checked metallographically. After the ingot was crushed to powders using a stainless steel (SUS 304) mortar and pestle, the powders were classified in diameter to less than 50 μm using screen analysis and analyzed using inductively coupled plasma-atomic emission spectrometry (ICP). The details of these experiments are shown elsewhere[82-83].

The milling process was stopped at regular intervals and a small amount of the milled powders was taken out from the vials in the glove box.

2.4. Analyses

The samples of the MA and MD processes were characterized as the function of the milling time by the following methods:

2.4.1. X-ray diffraction

Powder X-ray diffraction (XRD) data were obtained with Philips-Norelco and Rigaku diffractometers operating in the θ-2θ scan modes for MoKα radiation operated at 40 kV and 20 mA. The sample was placed on doubly sticky transparent tape mounted onto a microscope slide and placed in the area irradiated by X-ray (as determined using a KCl indicator). Standard silicon was used to calibrate the diffractometers. The X-ray data have a precision of 0.05 degree in 2 θ.

2.4.2. Thermal Analyses

The crystallization and amorphization behaviors of Al-TM amorphous alloys have been monitored by differential thermal analysis (DTA) and differential scanning calorimetry (DSC), respectively. The DTA measurements were performed on Rigaku at a heating rate of 0.33 Ks^{-1} in purified argon gas. In the DTA experiments, an amount (about 50 mg) of milled powders was inserted in a sample platinum pan. The lining of the pan was coated with α-Al_2O_3 to avoid any reactions between the samples (especially tantalum) and the platinum pan which could give false exothermic peak(s) especially at elevated temperatures. Further, a certain amount of α-Al_2O_3 (about 60 mg) was put into the reference platinum pan. Then, the pans were mounted on the holder of the DTA and the system was evacuated for about 7 ks using a diffusion pump. In the all measurements, the samples were heated up to 1400 K and cooled down about 400 K. Then the samples were reheated as second heating run to find the base line. X-ray diffraction was used to confirm the exothermic peaks.

On the other hand, the DSC experiments were performed on Seiko calorimeters interfaced to a microcomputer. The alloyed powders were sealed into aluminium pans. All the DSC measurements presented in this paper were carried out under in a flow of argon gas (0.83 mls^{-1}) at a heating heating rate of 0.67 Ks^{-1}. However, some alloyed powders had been heated at several heating rates to determine the activation energies of amorphization.

2.4.3. Metallography

The metallography of the alloyed powders has been studied by a scanning electron microscope (SEM) equipped with an electron probe microanalyzer (EPMA) operated at 20 kV and light optical microscope. In these experiments, a small amount of the alloyed powders was placed in a

plastic holder and wet ground carefully using fine silicon carbide emery papers (800-1500 mesh). The grinding was carried out by placing the emery paper on a flat glass plate and holding the specimen so that the scratches are formed in one direction only. Grinding is continued until the scratches left from the previous grinding operation are removed. The specimen is then swilled with ethanol and dried before being transferred to a finer paper. The grinding on the next emery paper is carried out so that the scratches are at right angles to those of the previous paper. Finally a series of fine scratches is obtained in the 1500 mesh grade of emery paper, and after washing and drying the specimen was ready for polishing. The grinding process was performed using paraffin as a lubricant to prevent particles of emery being embedded in the surface of the specimen. Then, the samples were polished on lapping tape (2000-6000 mesh) wetted by kerosene. Finally, the specimen was polished on silk cloth using a solution of white wax in benzene. Care was taken until a satisfactory surface was obtained without any distortions. Then, the specimen was etched using HCl (0.1 N) activated with five drops of H_2O_2 (10%). For the SEM observation, the samples were coated by gold, while the samples of the EPMA were coated by carbon.

2.4.4. Morphology

The morphology of the alloyed powders were examined by a 20 kV SEM and a 200 kV transmission electron microscope (TEM). For the SEM observations, a small amount of the powders was put on a copper holder coated by carbon dutite, whereas the samples for TEM observations were prepared by crushing the powders in ethanol. The samples had been dried before they were mounted on a copper microgrid.

2.4.5. Chemical analyses

The chemical analyses were performed using ICP interfaced to a microcomputer in order to detect exactly the contents of Al, TM metals and Fe contamination. For these analyses, an amount of the milled powders (about 30 mg) was dissolved in a leaching solution [HF(1N), 2 ml+H_2SO_4 (6N) 10 ml+HNO_3 (6N) 40 ml+H_2O_2 (36 wt.%) 2 ml] using a platinum container (100 ml in volume). Then, the solution was heated slowly until the powders dissolved completely without any precipitations. The solution was diluted with pure water in a volumetric mass flask (100 ml in volume). The ICP was calibrated by Al, Ti, Zr, Nb, Ta and Fe standard solutions before analyzing the sample. Each component for each sample was analyzed five times for more accuracy.

3. Results and Discussion

3.1. Preparation of amorphous Al_xTa_{1-x} alloy powders via BM and RM techniques

3.1.1. Structural change with the milling time

Figure 2 illustrates the XRD patterns of $Al_{30}Ta_{70}$ alloy powders after several milling time. The intensity of the Bragg-reflection peaks for pure Al and Ta decreases with increasing MA time. After 22 ks of milling time, the minor Bragg-peaks from Al (200), (220) and (311) reflections have disappeared. Moreover, the major Bragg-peaks from Al(111), (220) and (222) reflections, and from Ta (110), (200), (211), (220), (310) and (321) reflections decreased. Furthermore, these peaks become wider at the

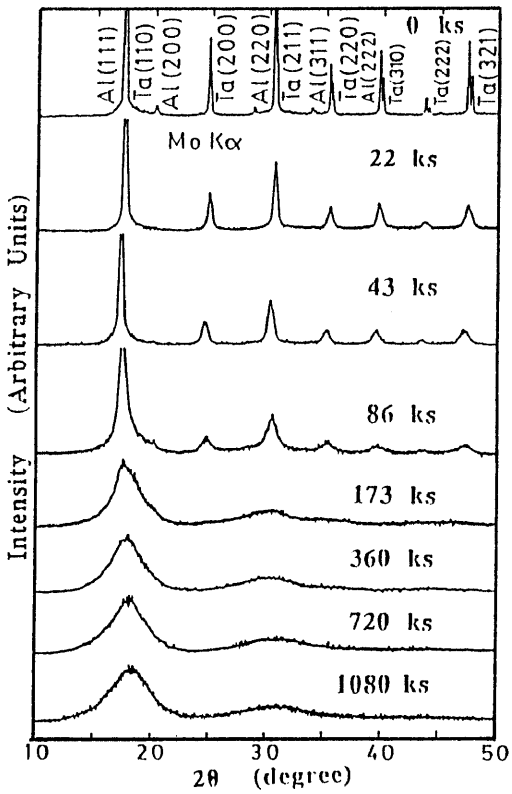

Fig. 2 XRD patterns of ball-milled $Al_{30}Ta_{70}$ alloy powders as a function of the MA times.

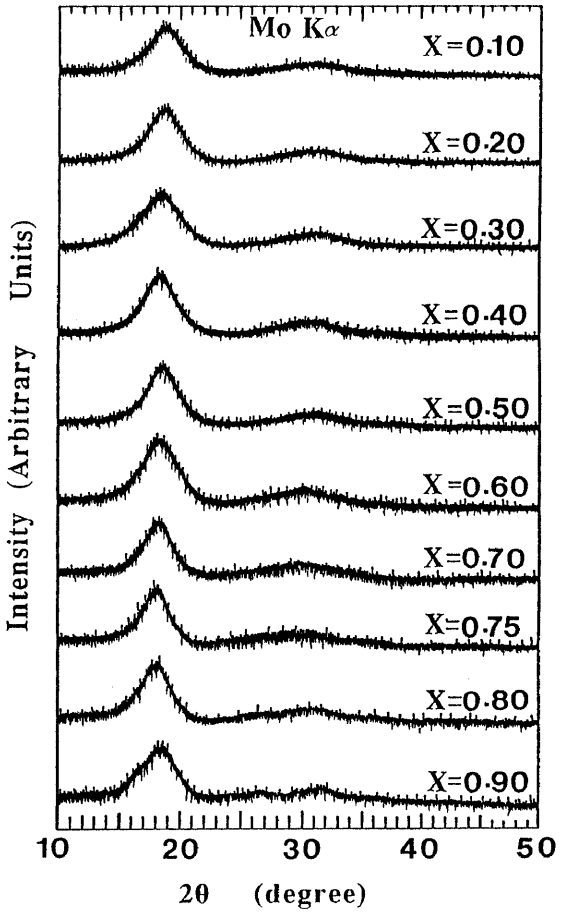

Fig. 3 XRD patterns of ball-milled Al_xTa_{1-x} alloy powders after 1080 ks of the MA time.

end of the early stage of milling (86 ks). An amorphous phase is obtained after 173 ks, characterized by visible halo pattern. Towards the end of BM process (720 to 1080 ks), this peak is progressed in becoming broad and smooth.

The XRD patterns of Al_xTa_{1-x} ($0.10< x <0.90$) after the final stage of BM, i.e. 1080 ks are shown in Fig.3. At this stage of milling, clear halo-diffraction patterns are shown, indicating the formation of amorphous Al_xTa_{1-x} alloy powders in the range of $0.10< x <0.75$.

3.1.2. Thermal analysis for ball milled Al_xTa_{1-x} alloy powders

The thermal properties, i.e. crystallization temperature (T_x) and enthalpy of crystallization (ΔH_x) of Al_xTa_{1-x} amorphous alloy powders have been investigated by DTA method. Figure 4 shows the DTA curves of $Al_{30}Ta_{70}$ alloy powders after several BM times. After 173 ks of milling, a rather broad single exothermic peak appears at about 1000 K. This exothermic reaction occurs as a result of amorphous-crystalline transformation in the alloy powders. Obviously, the exothermic peak becomes more pronounced and sharper with increasing the MA time, indicating that the amorphous phase becomes more homogeneous being contains single phase. Moreover, this peak shifts to the elevated temperature with increasing the BM time, suggesting a compositional change of the mechanically alloyed powders. Towards the end of BM process (720 to 1440 ks), the onset temperature of this exothermic peak approaches to saturation value as a high as 1120 K, as shown in Fig.4.

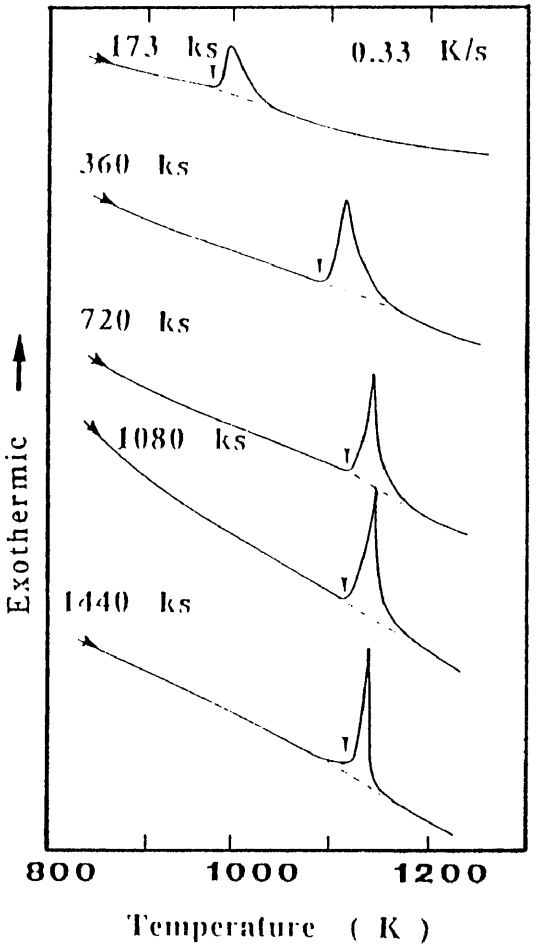

Fig. 4 Typical DTA curves of ball-milled $Al_{30}Ta_{70}$ alloy powders after selected MA times.

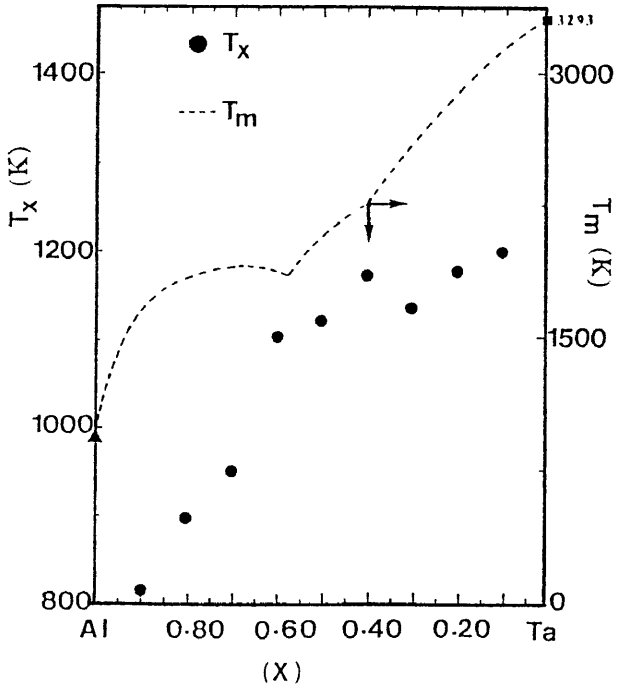

Fig. 5 Crystallization temperature, T_x, of ball-milled Al_xTa_{1-x} alloy powders after 1080 ks of the MA time as a function of Al content, x.

Figure 5 illustrates T_x of mechanically alloyed Al_xTa_{1-x} powders after the final stage of milling (1080 ks). It is shown that T_x increases in roughly parallel with the melting points (T_m) as the Ta content increases. It is worth noting that T_x is a maximum near the equilibrium composition (43 at.% Ta). The ratio of T_x/T_m for amorphous Al_xTa_{1-x} binary alloy powders is shown in Fig.6. The amorphization range of Al_xTa_{1-x} depends strongly on this ratio, i.e. when this ratio is between 0.4 and 0.65 a homogeneous single-amorphous phase is obtained, and the amorphization reaction occurs easy. On the other hand, when it is below than 0.4, the formed phase is either crystalline or amorphous-crystalline phases, as shown in Fig.6.

Figure 7 illustrates ΔH_x of mechanically alloyed Al_xTa_{1-x} powders after 1080 ks of BM. ΔH_x was calculated from the area under the exothermic peak of crystallization. The enthalpy of formation (ΔH_{for}) was calculated according to Miedema's model [80-81] and plotted in Fig. 7 (dashed line). The absolute value of ΔH_x is maximum (21 kJ/mol) near the stoichiometric compound $AlTa_2$ in which crystallization happens easily without long distance diffusion of constituent atoms[22].

3.1.3. Chemical analysis

The iron contamination content in the end-product (1080 ks) of ball-milled Al_xTa_{1-x} powders is shown in Fig.8. As the Ta content in the alloyed powders increases, the iron contamination content increases. This is attributed to the formation of Ta-Al as a hard refractory alloys. Therefore, MA process via BM must lead to high concentration of iron due to ball-powder-ball collision: this is a natural consequence of the collision between milling media. Therefore, MA process are faced with this serious problem which has impeded progress. Since the ball-powder collision can be considered as the main source of iron contamination, we have to use different kind of

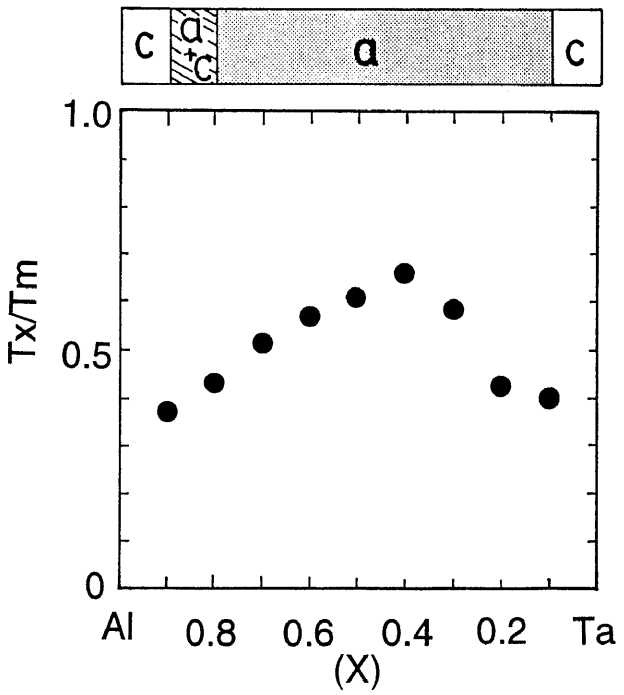

Fig. 6 Dependence of T_x/T_m on Al content, x, of ball-milled Al_xTa_{1-x} alloy powders after 1080 ks of the MA time The range of amorphization is presented by "a", whereas, "c" presents the crystalline phase(s).

tumbling mills in which there is no collision between the milling media, that is to say, rod-mill (RM).

Figure 9 shows the amount of iron contamination in mechanically alloyed $Al_{30}Ta_{70}$ powders as a function of (a) RM and (b) BM times, as well as the effect of repeating the MA process. At the beginning of the first milling run the milling media were used in the absence of mechanically alloyed powder coatings. After this run the milling media which had been coated by the powders were used again in the second and third runs without removing the coated powder. A drastic decrease in iron content from the first to the third milling runs was observed. It is also shown that the amount of iron contamination in the rod-milled powders (less than 1 at.%) is lower than in the ball-milled powders (about 2 at. %).

3.1.4. Thermal analysis for ball milled and rod milled $Al_{30}Ta_{70}$ alloy powders

Figure 10 illustrates the DTA curves for $Al_{30}Ta_{70}$ alloy powders after selected (a) RM and (b) BM times. All of the samples were cooled to about 400 K after heating to 1250 K. The samples were then reheated in a second heating run (dashed line) in order to obtain a base line. As illustrated, single exothermic peaks were observed. In RM alloys (a) a sharp exothermic peak is observed after 720 ks of the milling time, indicating the formation of a homogeneous amorphous phase. In BM alloys (b), however, a broad exothermic peak is shown after the same milling time (720 ks) suggesting the formation of a heterogeneous amorphous phase. The arrows in the curves refer to the onset T_x. ΔH_x was evaluated from the area under each exothermic peak for all rod-milled and ball-milled samples.

Figure 11 shows (a) ΔH_x and (b) T_x for rod-milled (solid curves) and ball-milled (dashed curves) $Al_{30}Ta_{70}$

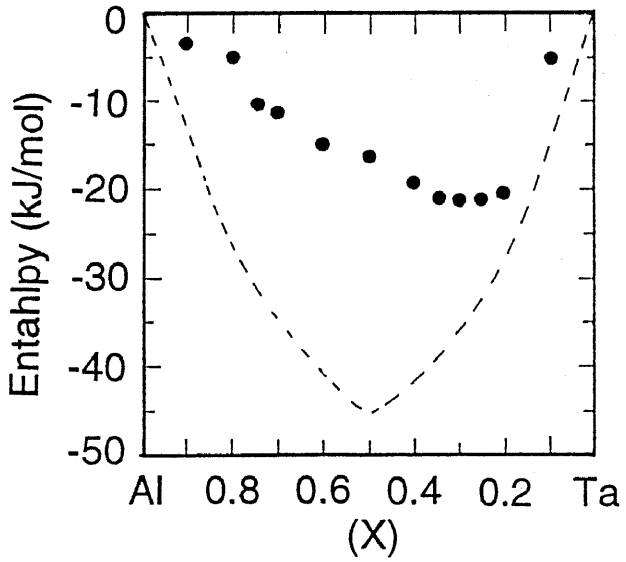

Fig. 7 Enthalpy change of crystallization, ΔH_x, of ball milled Al_xTa_{1-x} alloy powders after 1080 ks of the MA time as a function of the MA time. The dashed line presents the enthalpy of formation, ΔH_{for}, calculated from Miedema's model (refs. 80, 81).

alloy powders after several milling times. The ΔH_x decreases sharply during the early and intermediate stages of milling (22 to 360 ks), suggesting a drastic conversion to the amorphous state. At the final stage of milling (720 to 1440 ks) the ΔH_x approaches a saturation value. The dependence of T_x on RM and BM time for mechanically alloyed $Al_{30}Ta_{70}$ powders is shown in Fig. 11(b). With increasing the milling time T_x increases drastically in the early and intermediate stages of milling and approaches a saturation value after the final stage of milling, 1440 ks. It is worth noting that T_x of rod-milled $Al_{30}Ta_{70}$ alloy powders (1216 K) is higher than that one for ball-milled $Al_{30}Ta_{70}$ alloy powders (1170 K), suggesting that RM technique leads to the formation of amorphous alloy powders with a high thermal stability. This is caused by the low impurity contamination and high homogeneity in the formed rod-milled alloy powders.

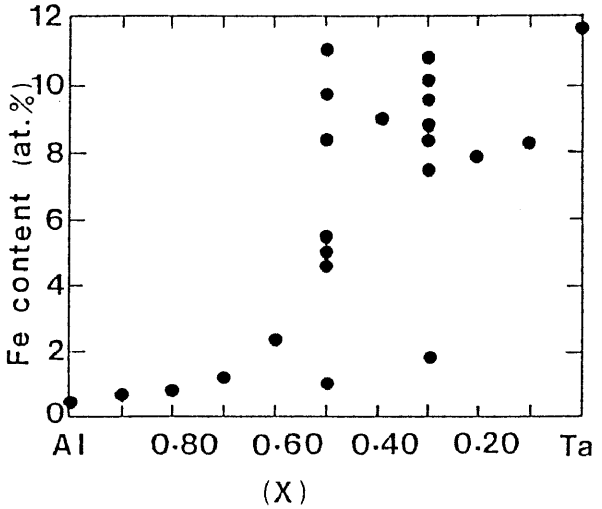

Fig. 8 Iron contamination content in the end-product, 1080 ks, of ball-milled Al_xTa_{1-x} alloy powders as a function of Al content, x.

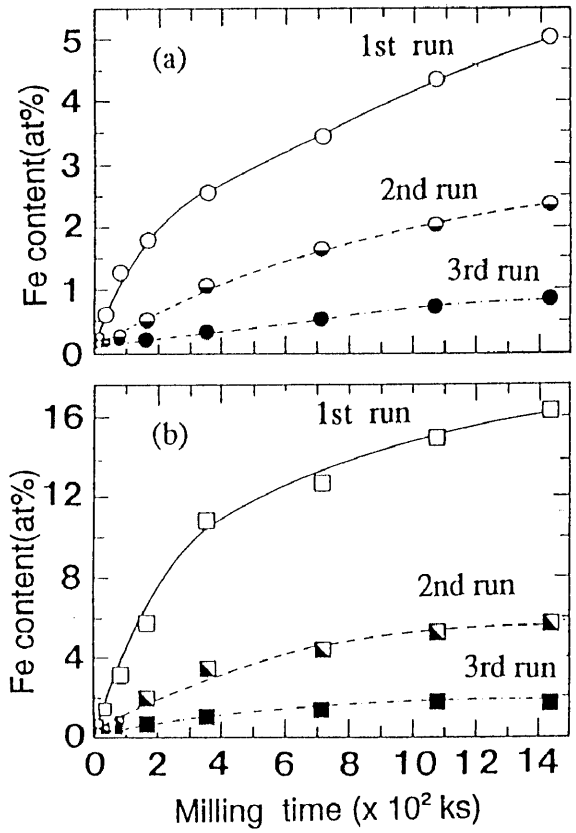

Fig 9 Iron contamination content in (a) rod-milled and (b) ball-milled $Al_{30}Ta_{70}$ alloy powders as a function of milling technique, milling times and repetition of milling process.

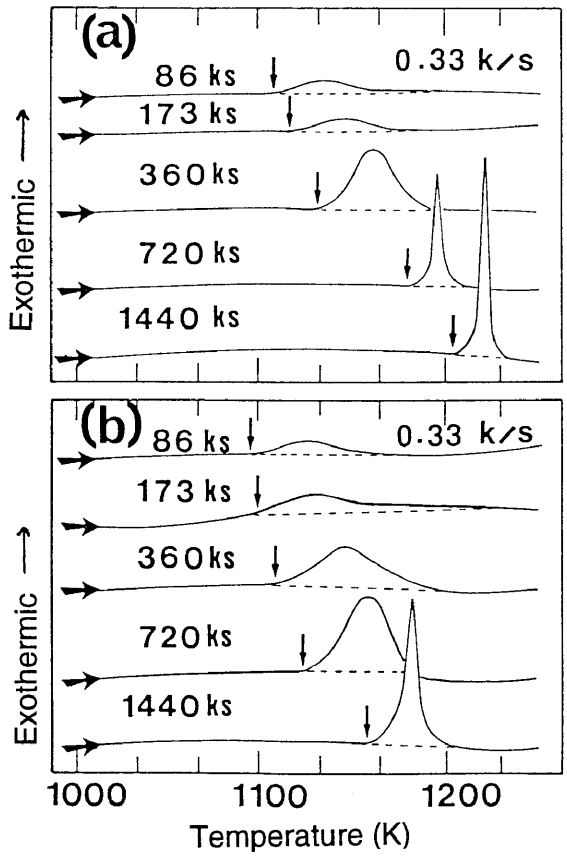

Fig. 10 DTA curves for mechanically alloyed $Al_{30}Ta_{70}$ powders as a function of (a) rod-milling and (b) ball-milling times.

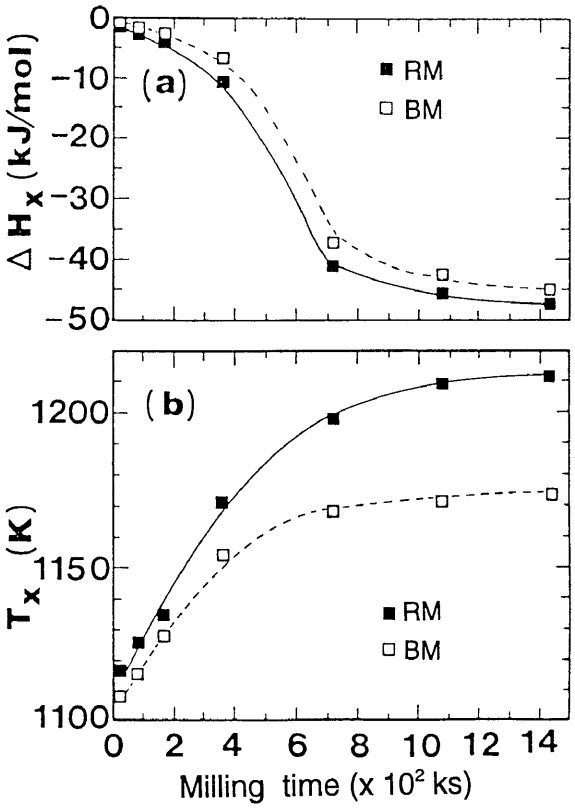

Fig. 11 Enthalpy change of crystallization, ΔH_x, and crystallization temperature, T_x, of $Al_{30}Ta_{70}$ alloy powders as a function of the rod-milling, RM and ball-milling, BM, times.

3.1.5. Morphology ball milled and rod milled $Al_{30}Ta_{70}$ alloy powders

Figure 12 presents the optical micrographs of polished particles of $Al_{30}Ta_{70}$ alloy after 43 ks of (a) RM and (b) BM times. At this stage of MA time, the individual particles are layered. It is worth noting that RM leads to formation of powder particles contain many layers of elemental Al and Ta in good arrangement as a result of the applied shear force. In BM powder particles, however, the layered-structure morphology appears in a haphazard arrangement as a result of the impact force which leads to formation of particles with random arrangement of the layered-structure, as shown in Fig.12(a). In fact, the solid-state amorphization reaction is usually triggered by the solid-state binding between fresh surfaces of the constituent metals. The shear due to the colliding force must therefore be stronger than the impact in the MA process for amorphous alloy formation. In principle the RM technique is more suitable for the effective application of shear force than conventional BM technique.

The particle size distribution of mechanically alloyed $Al_{30}Ta_{70}$ powders via RM (closed symbols) and BM (open symbols) techniques is presented in Fig.13 as a function of the milling time. In the BM process the starting elemental powders usually agglomerate at the early stage of milling to form powders of greater diameter, as large as several hundred microns, and this is followed by continuous disintegration until the particle size is less than a few microns. RM leads to a similar behavior for the variation in powder diameters. In RM, however, the average diameter of the agglomerate powders is very small and subsequent disintegration into fine powders proceeds at high rate to provide a narrow size distribution.

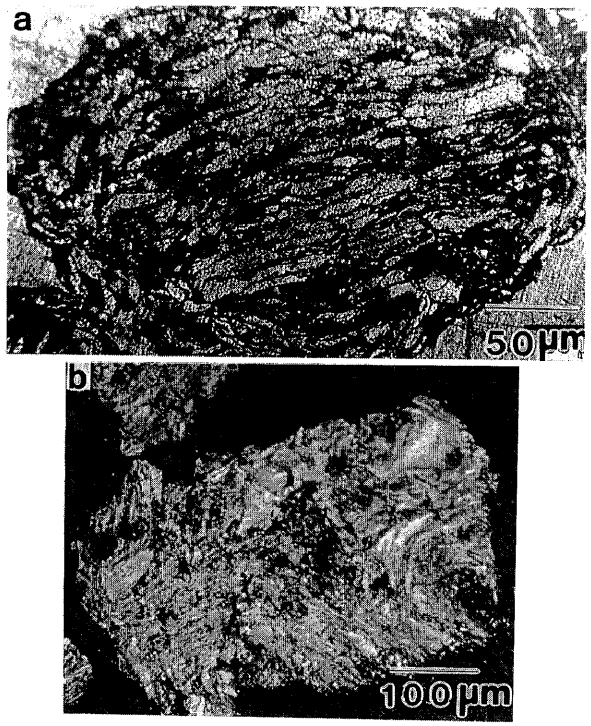

Fig. 12 Cross-sectional view of the individual particles of mechanically alloyed $Al_{30}Ta_{70}$ powders after 43 ks of (a) rod-milling and (b) ball-milling times.

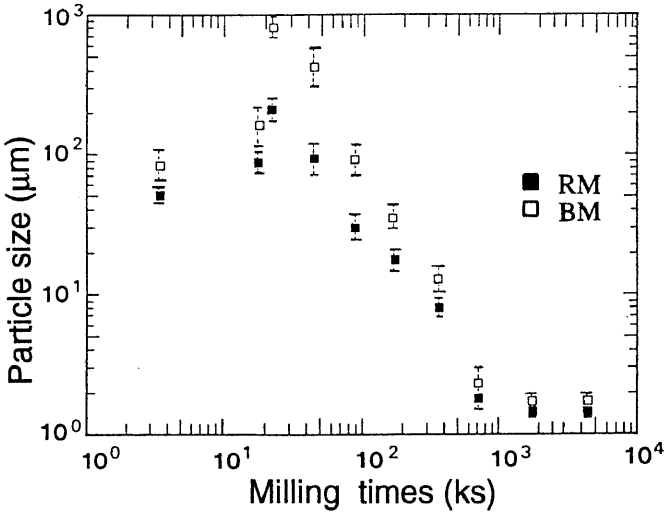

Fig. 13 Particle size distribution of mechanically alloyed $Al_{30}Ta_{70}$ powders as a function of the rod-milling, RM (closed symbols) and ball-milling, BM (open symbols) times.

3.2. Preparation of amorphous $Al_{50}TM_{50}$ (TM; Ti, Zr, Nb and Ta) alloy powders via RM technique

3.2.1. Structural Evolutions

Figure 14 illustrates the XRD patterns of rod-milled $Al_{50}TM_{50}$ alloy powders after the final stage of milling, 1440 ks. The broad haloes suggest the formation of an amorphous phase. The XRD patterns of $Al_{50}TM_{50}$ alloy powders as a function of the MA times have been shown in previous work[24,72,82].

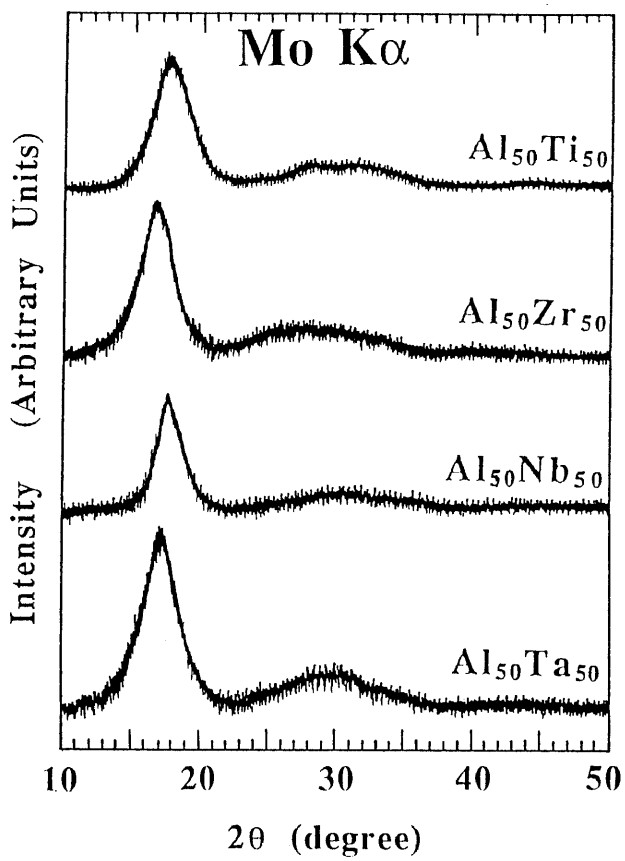

Fig. 14 XRD patterns of rod-milled $Al_{50}TM_{50}$ (TM; Ti, Zr, Nb and Ta) alloys after the final stage of the MA time, 1440 ks.

3.2.2. Morphology

3.2.2.1. SEM observations and optical microscopy

For the purposes of this study, detailed optical and SEM observations are performed to determine the structure, shape and size of $Al_{50}Zr_{50}$ alloy powders (as a typical example) during the different stages of milling. Figure 15 shows the SEM micrographs of rod-milled $Al_{50}Zr_{50}$ alloy powders after selected milling time. The particles in the first stage of rod-milling, exemplified by the 11 ks and 43 ks alloy powders are shown in Figs.15(a) and 15(b), respectively. At the first few ks of milling (2 to 11 ks) the rods and the shell wall are completely coated by a thick welded layers of the starting elemental powders. After 11 ks of the MA time, the particles have a globe shape with cabbage or orange skin-like morphology, as shown in Fig.15(a). Further milling (43 ks) leads to the formation of particles with greater diameters, as large as 1000 μm, as shown in Fig.15(b). The optical metallographic view of the cross-section for the powders shows that the individual particles contain many fine layers with thickness that vary from 10 to 20 μm, as shown in Fig.16(a). For longer milling times, these layers become hardly visible even by SEM after 260 ks, as shown in Fig.16(b). Moreover, the powders disintegrate and become finer with size less than 10 μm in diameter, as shown in Fig.15(c). At the end of the rod-milling process (1440 ks) the powder particles become uniform in size (less than 1 μm in diameter) and have spherical-like morphology, as shown in Fig.15(d). It is worth to say that the coated material is removed from the milling tools during this stage of milling, because the amorphous alloy powders are not ductile and more brittle than the elemental powders.

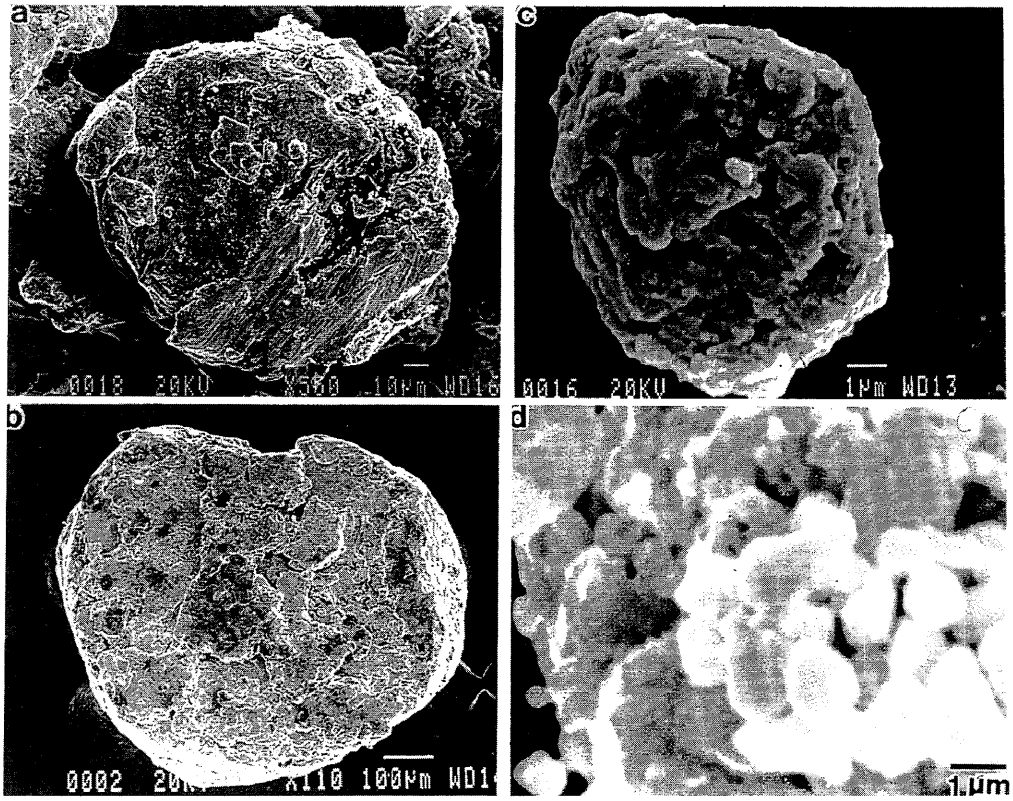

Fig. 15 SEM micrographs of rod-milled $Al_{50}Zr_{50}$ alloy powders after 11 ks(a), 43 ks(b), 173 ks(c) and (d) 1440 ks of the MA times.

Figure 17 summarizes the SEM observations of rod-milled $Al_{50}TM_{50}$ alloy powders at the different stages of milling. Obviously, the MA process performed by the rod-milling technique can be classified into three stages, that is to say, agglomeration, disintegration or amorphization and homogenization stages. In the agglomeration stage (0 to 43 ks) the elemental powders of Al and TM are agglomerated and grow in their sizes as a result of the repeated cold welding. During this stage of milling, the powders vary widely in size from 100 to 1000 μm. During the subsequent disintegration stage (43 to 360 ks) which can be also called as amorphization stage, the agglomerated powder particles are subjected to a continuous disintegration with fragmentation to form finer powders with size less than 10 μm in diameter. Furthermore, this stage of milling provides powder particles with narrow size distribution. The homogenization stage (360 to 1440 ks) may be refer to the last stage of rod-milling in which all the powders are uniform in shape and size. In addition, this stage of milling provides fine powders, as fine as 1 μm in diameter.

It is worth mentioning that the MD process leads to a different behavior for the variation in powder diameters, as illustrated in Fig.18. The starting powders of AlTa intermetallic compound are continuously reduced in size without any agglomerations or to form fine powders with about 10 μm in diameter after only 22 ks, as shown in Fig.18(d). In addition, the layer-structure morphology is absent, as shown in Fig. 19. This is because the starting material of MD is a compound by itself. At the final stage of milling, the particle size states of the MA and MD $Al_{50}Ta_{50}$ alloy powders is nearly the same in size, as shown in Fig.20. Furthermore, the amorphization process in the MD occurs through a single stage, as shown in

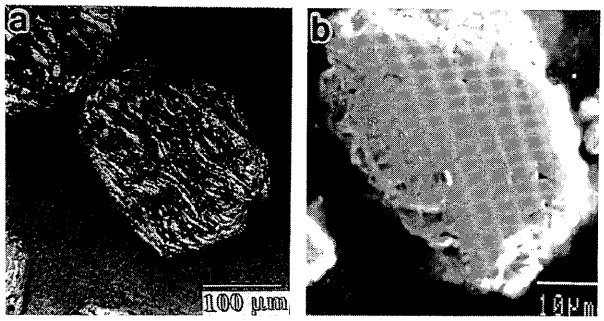

Fig. 16 Cross-sectional view of the polished powder particles of rod-milled $Al_{50}Zr_{50}$ alloy after (a) 86 ks and (b) 260 ks of the MA times.

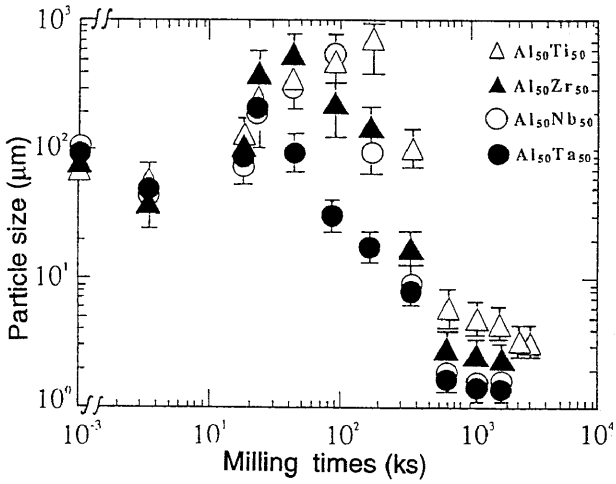

Fig. 17 Particle size distribution of rod-milled $Al_{50}TM_{50}$ (TM; Ti, Zr, Nb and Ta) alloy powders as a function of the MA times and TM elements.

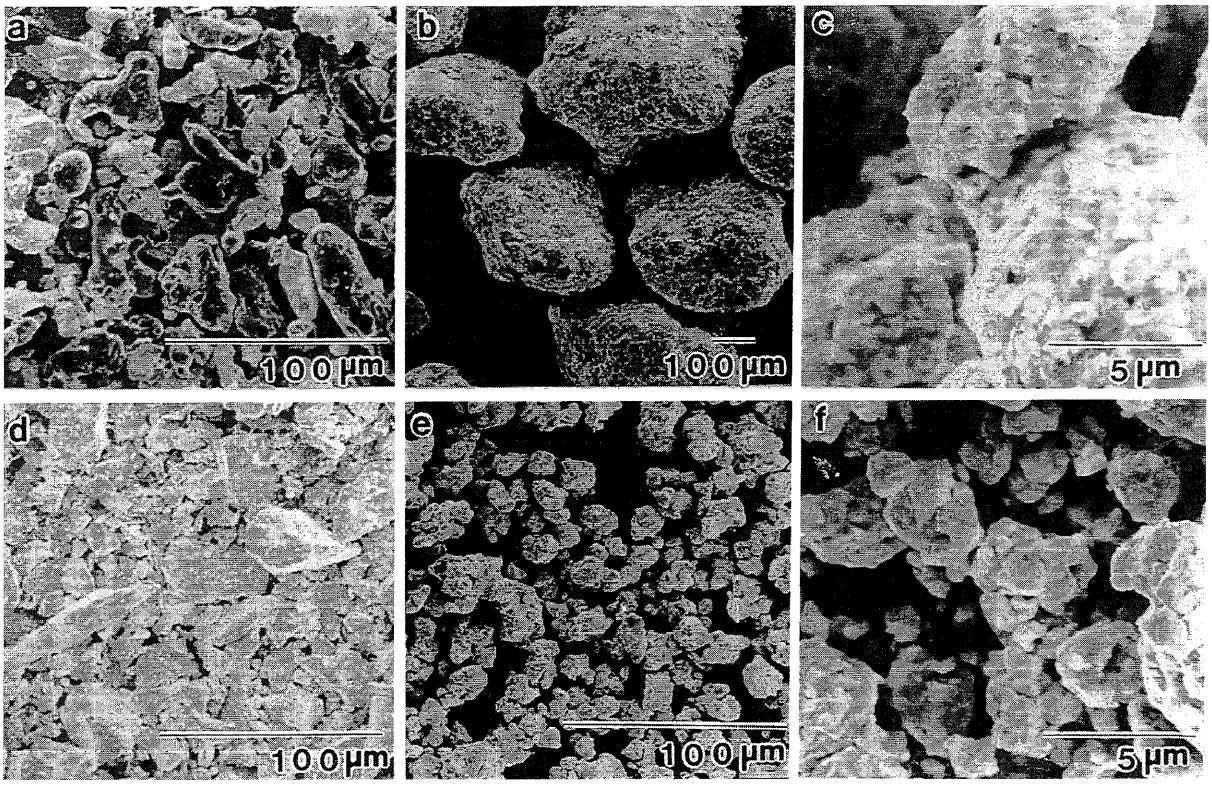

Fig. 18 SEM micrographs of rod–milled $Al_{50}Ta_{50}$ alloy powders mechanically alloyed(MA) for 0 ks (a), 22 ks (b) and 360 ks (c), and mechanically disordered(MD) for 0 ks (d), 22 ks (e) and 360 ks (f).

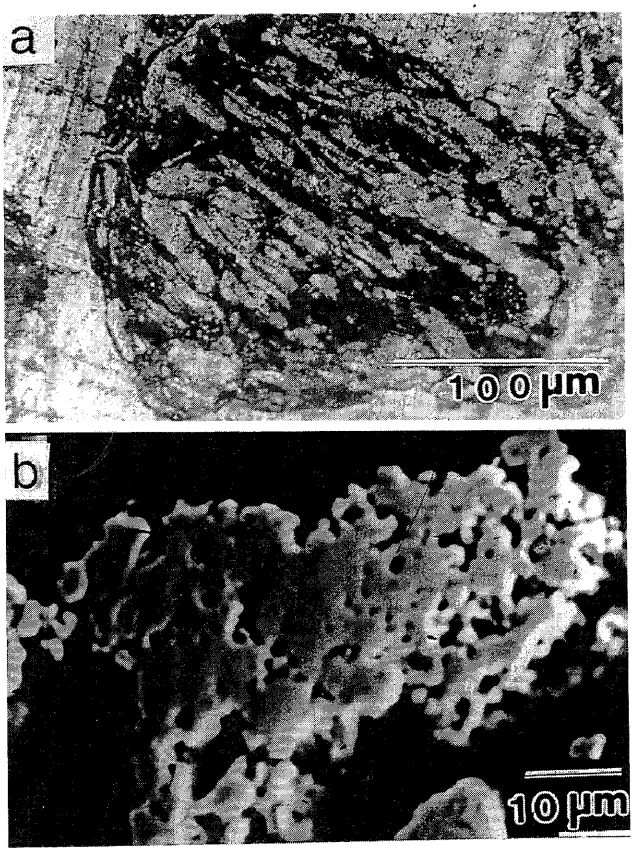

Fig. 19 Cross-sectional view of the polished powder particles of rod-milled $Al_{50}Ta_{50}$ alloy after 22 ks of (a) MA and (b) MD times.

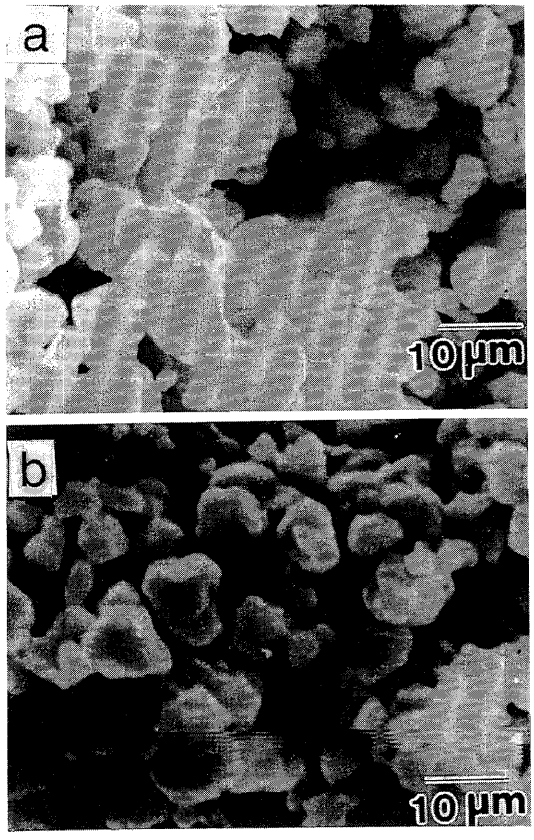

Fig. 20 SEM micrographs of the end-product of $Al_{50}Ta_{50}$ alloy powders after 1440 ks of (a) MA and (b) MD times.

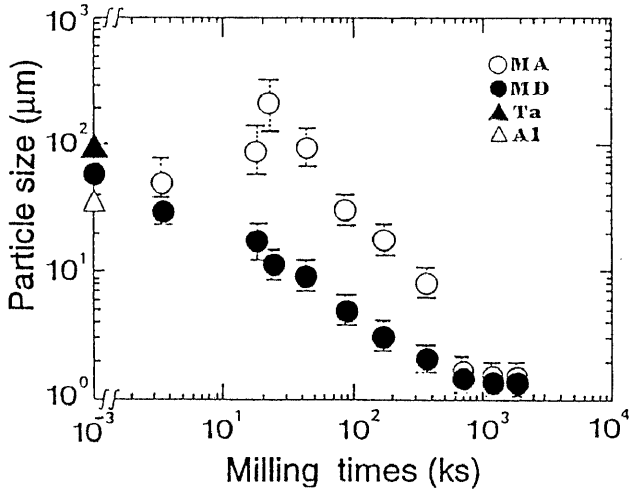

Fig. 21 Particle size distribution of rod-milled $Al_{50}Ta_{50}$ alloy powders as a function of the MA (open symbols) and MD (closed symbols) times.

Fig.21. Obviously, the size reduction of the particles proceeds at a high rate to provide homogeneous powder particles with narrow size distribution[83].

3.2.2.2.TEM observations

In order to reveal much more information, the amorphization progress via the rod-milling technique has been investigated by TEM and EDX. The TEM/EDX technique provide information on the structure and the composition of the powder particles in very small areas (less than 50 nm in diameter). Moreover, this technique allow us to distinguish between the crystalline and the amorphous phase in which SEM is not able to give such information.

Figure 22 shows the bright-field images (BFI) and the selected-area diffraction patterns (SADP) of rod-milled $Al_{50}Zr_{50}$ alloy powders at the agglomeration and disintegration stages of the MA process. After 11 ks of rod-milling, the powder particles are heavily faulted, characterized by parallel rows of faults which appears as multiple fringes. The SADP shows a sharp ring-spot pattern that is characteristic of several simultaneity diffracting polycrystalline Al(fcc) and Zr(hcp). It is worth mentioning that there is no evidence of the formation of an amorphous phase in this stage of milling. The BFI, the dark-field image and the corresponding SADP for rod-milled $Al_{50}Zr_{50}$ alloy powders after 43 ks of the MA time. The crystalline sizes are distributed between 10 and 20 nm. The alloy powders contain polycrystalline Al/Zr crystals, characterized by several sharp ring-spot pattern, as shown in Fig.23(c).

Figure 24 shows the BFI near the edge of a particle for $Al_{50}Zr_{50}$ alloy milled for 173 ks (disintegration stage). Increasing the MA time leads to increasing the shear force by the rods and this causes mechanical deformation on the powder particles which translated into numerous faults and dislocations appear clearly in regions I and II, as shown in Fig.24. Contrary to this, the region III has a fine and somewhat uniform structure which indicates the existence of an amorphous phase, characterized by a halo-diffraction pattern, as shown in SADP (III). Moreover, the structure of the alloy powders is extremely heterogeneous, shown by the different features of SADPs taken at regions I (unprocessed Zr), II (unprocessed Al) and III (amorphous AlZr).

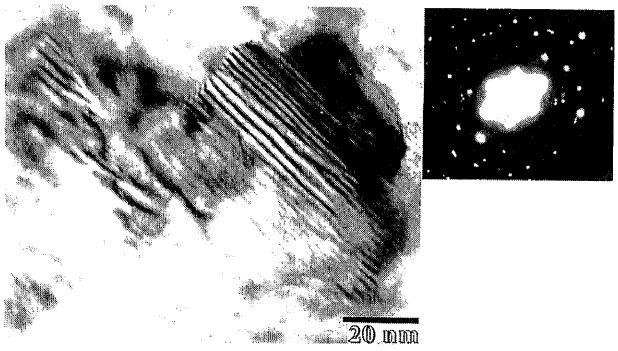

Fig. 22 The bright-field image and the corresponding diffraction pattern of rod-milled $Al_{50}Zr_{50}$ alloy powders after 11 ks of the MA time.

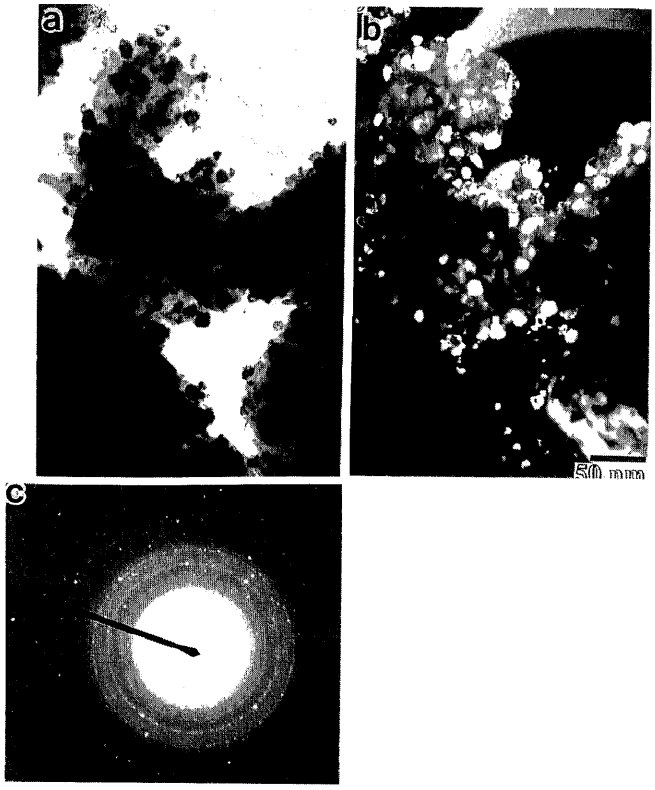

Fig. 23 The bright-field image (a), dark-field image (b) and the corresponding diffraction pattern (c) of rod-milled $Al_{50}Zr_{50}$ alloy powders after 43 ks of the MA time.

The BFI and the corresponding SADP of center particle for the end-product $Al_{50}Zr_{50}$ alloy powders (1440 ks) are shown in Fig.25. Overall, the sample appears to have a homogeneous fine structure with no dominant facet structure. Moreover, the SADP shows a typical halo-pattern of an amorphous phase in good agreement with the previously published X-ray diffraction patterns[72].

3.2.3. Thermal Analysis

Figure 26 illustrates the typical DTA curves for the rod-milled $Al_{50}Zr_{50}$ alloy powders as a function of the MA time. All the samples were heated to about 1200 K (first run) and cooled down to about 600 K. Then, second heating runs (dashed lines) were performed in order to get a base line. The DTA curves of the alloy powders at the agglomeration stage of milling are shown in Fig.26(a).

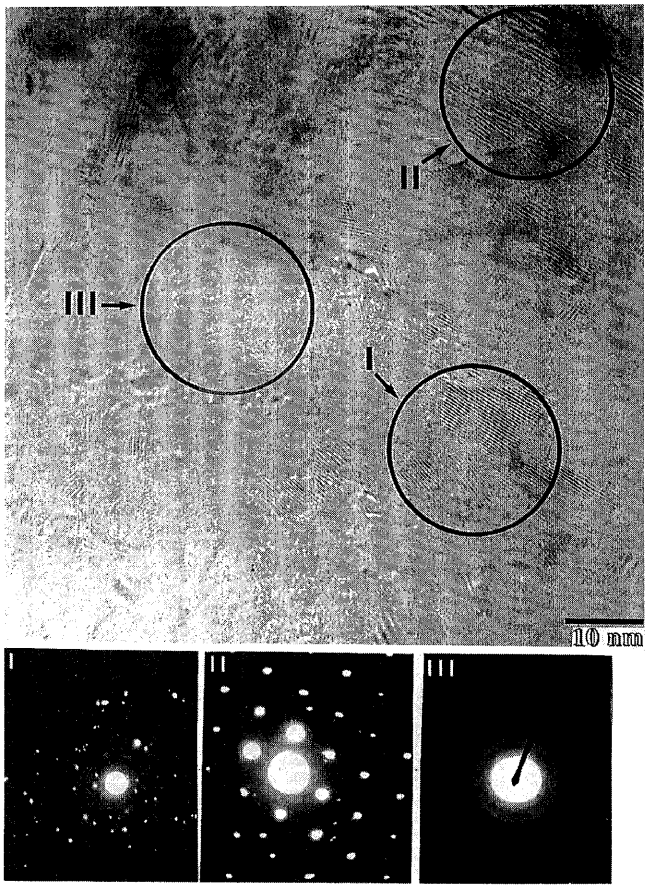

Fig. 24 High magnification bright-field image and the corresponding diffraction patterns of rod-milled $Al_{50}Zr_{50}$ alloy powders after 173 ks of the MA time.

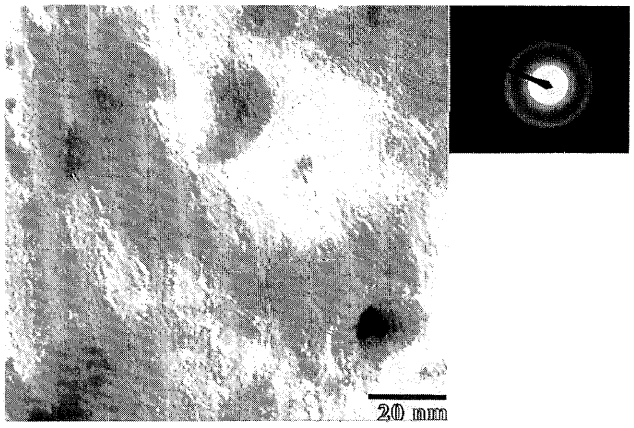

Fig. 25 The bright-field image and the corresponding diffraction pattern of rod-milled $Al_{50}Zr_{50}$ alloy powders after 1440 ks of the MA time.

During this stage of milling, a sharp endothermic peak appears at about 930 K due to the melting of pure Al in the starting material of $Al_{50}Zr_{50}$ powders. The melt then reacts with elemental Zr powders in the mixture, characterized by an exothermic peak appears above to 1100 K. After 43 ks of milling, however, the endothermic and exothermic reaction peaks had already disappeared and two broad exothermic peaks appear. The peak temperature of the first exothermic peak does not change with further milling, as shown in Fig.26(b).

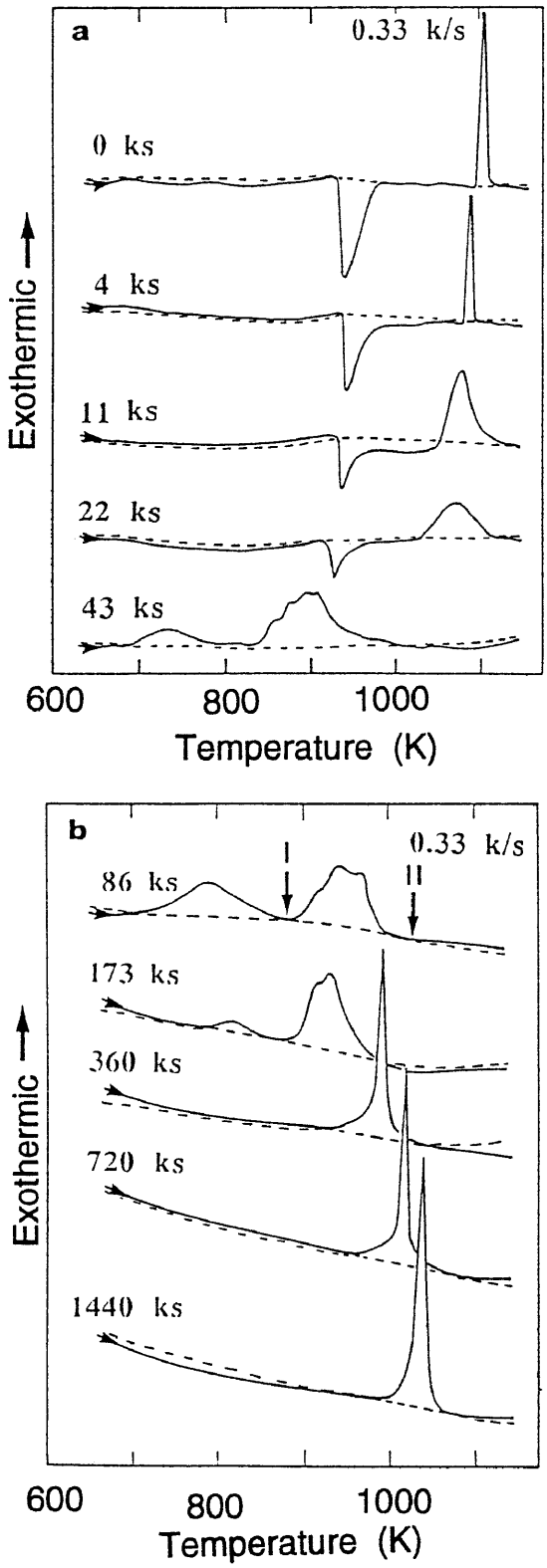

Fig. 26 DTA curves for rod-milled $Al_{50}Zr_{50}$ alloy powders at (a) the agglomeration stage and (b) during the amorphization and homogenization stages of the MA times.

In order to identify the origin of these exothermic reactions, two samples of 86 ks mechanically alloyed powders were heated separately in the DTA for TEM investigations at (I) and (II), as presented in Fig.26(b). The TEM observations have allowed direct imaging of the

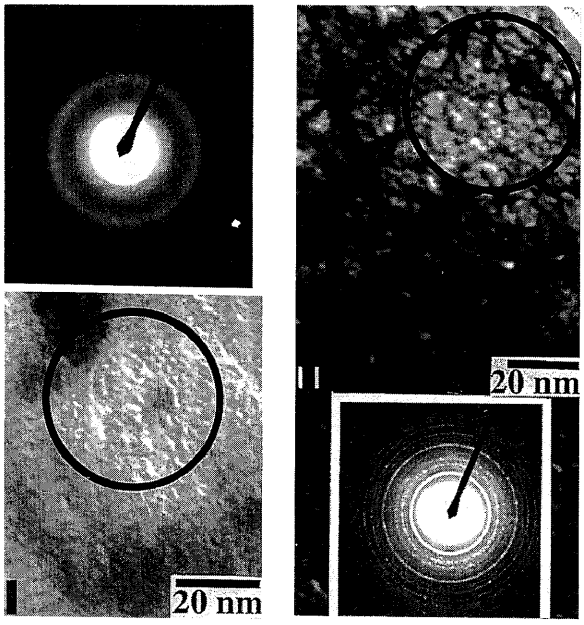

Fig. 27 TEM images and the corresponding diffraction patterns of rod-milled $Al_{50}Zr_{50}$ alloy powders milled for 86 ks, then heated to (I) 880 K and (b) 1025 K.

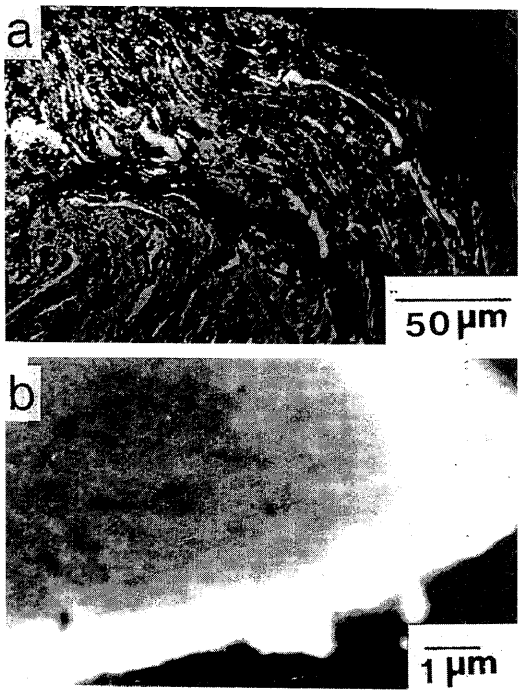

Fig. 29 Cross-sectional view of $Al_{50}Ti_{50}$ alloy powders milled for 173 ks of the MA time, then heated to (a) 400 K and (b) 680 K.

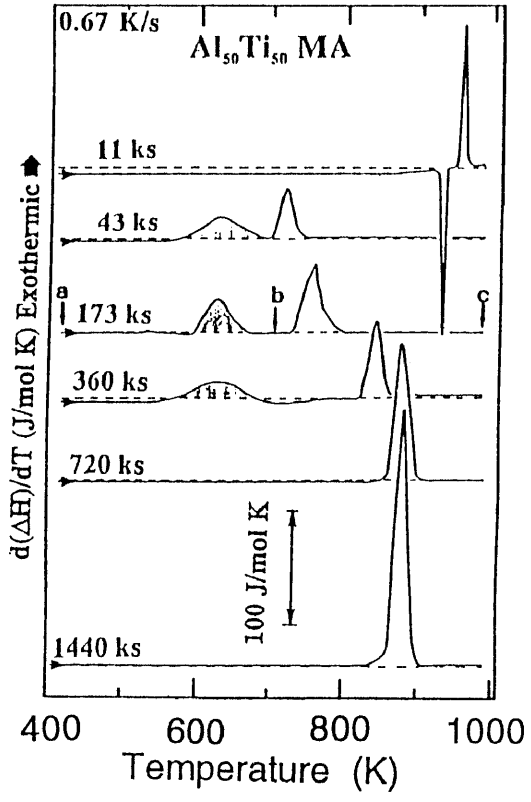

Fig. 28 DSC curves for mechanically alloyed $Al_{50}Ti_{50}$ alloy powders as a function of the rod-milling times.

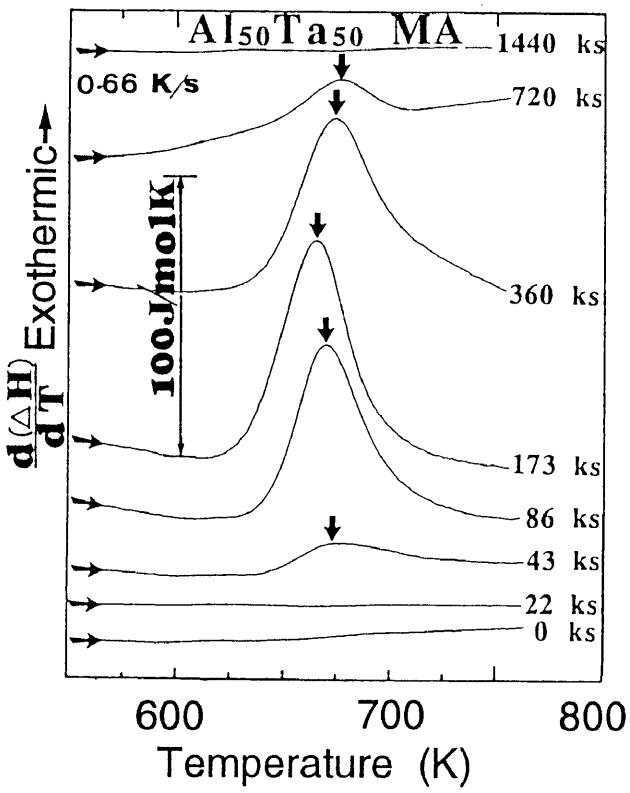

Fig. 30 DSC curves of the amorphization peak for rod-milled $Al_{50}Ta_{50}$ alloy powders after several stages of the MA times.

phase formation for these samples. Figure 27 shows TEM images that were obtained from as heated alloy powders to 880 K (I) and 1025 K (II), respectively. The BFI and SADP of the sample (I) heated to 880 K indicate the formation of an amorphous phase, characterized by the featureless image and clear halo-pattern, as shown in Fig.27(I). Consequently, it is concluded that the first exothermic peak is due to the transformation from the crystalline to amorphous state, i.e. the thermally assisted solid state amorphization reaction (TASSA). It is worth to say that the formation of the amorphous phase in this stage of milling (86 to 360 ks) occurs mainly due to the TASSA. The sample (II) taken at 1025 K, however, shows at all regions without any exceptions, sharp ring-spot

pattern, as shown in Fig.27(II). The ring pattern, which can be indexed as polycrystalline AlZr is characteristic of crystallization of the amorphous phase.

The peak temperature of the second exothermic peak shifts to the elevated temperature at the amorphization and homogenization stages of milling, as shown in Fig.26(b). Towards the end of the MA time, the second exothermic peak becomes pronounced and sharp, suggesting the formation of a homogeneous amorphous phase.

Same observations have been found in the other Al-TM binary systems, exemplified by $Al_{50}Ti_{50}$ alloy powders, as shown in Fig.28. In order to examine the microstructural changes of the particles before and after the amorphization peak, two samples of 173 ks $Al_{50}Ti_{50}$ alloy powders were taken at a and b, as shown in Fig. 28. The sample (a) which was heated at 400 K (far below the amorphization peak) has a layered-structure morphology, as shown in Fig.29(a). These layers of elemental Al and Ti disappear in the sample (b) heated to about 680 K (well above the amorphization peak), as shown in Fig.29(b).

The DSC curves for low temperature range (500 to 800 K) of MA $Al_{50}Ta_{50}$ alloy powders are shown in Fig.30 as a function of the milling time. The DSC has been used to get the values of the amorphization temperature, T_a, the activation energy of amorphization, E_a, and the enthalpy change of amorphization, ΔH_a, with more accuracy. Obviously, the amorphization peak, appears at about 680 K, after 43 ks of MA time. After 173 ks of milling time, the peak becomes more pronounced. Then, this amorphization peak gradually disappears to be not remarked after 1440 ks of MA time. The DSC curves for the amorphization peaks of the other Al-TM binary systems had already published elsewhere[25,72].

The values of E_a for rod-milled $Al_{50}TM_{50}$ alloy powders after 173 ks of milling was determined by Kissinger method and shown in Fig.31. The parameters T_P and Φ refer to the temperature of the amorphization peak and the heating rate, respectively. The values of E_a were calculated from the slope of the line to be 168, 156, 179

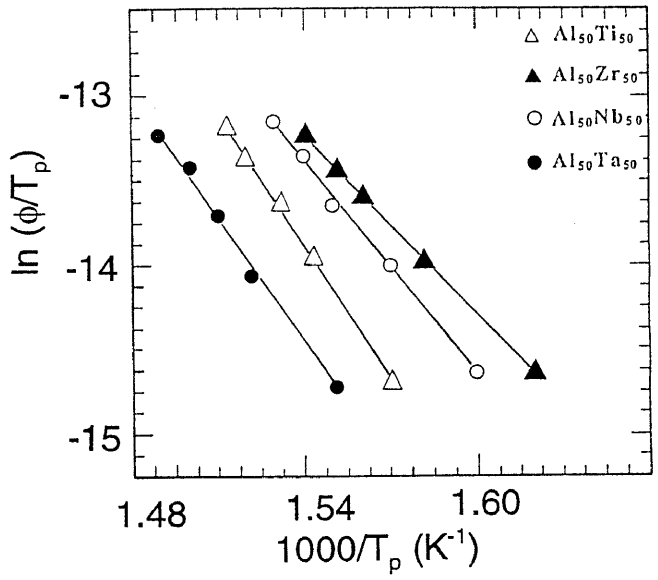

Fig. 31 Kissinger plot of amorphization for rod-milled 173 ks $Al_{50}TM_{50}$ (TM; Ti, Zr, Nb and Ta) alloy powders.

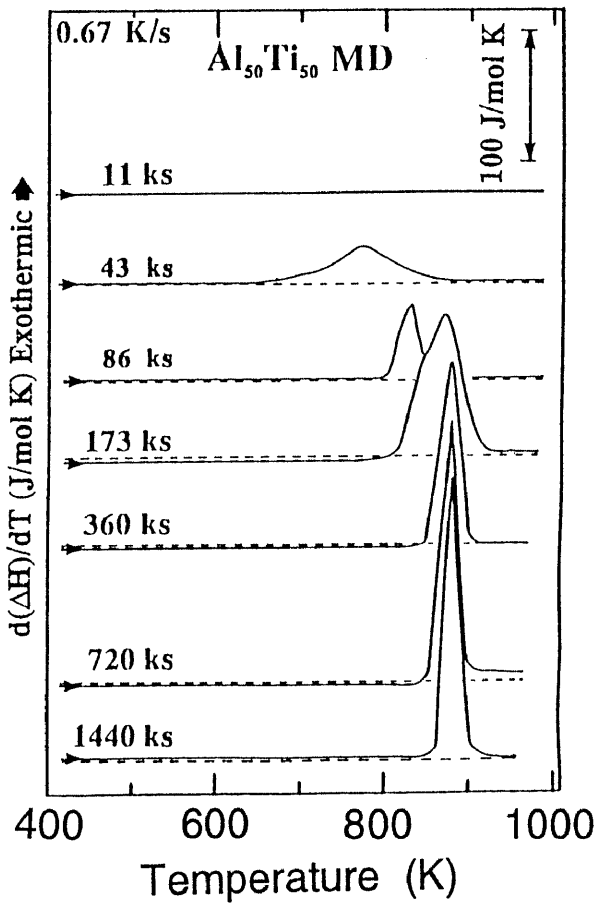

Fig. 32 DSC curves for rod-milled $Al_{50}Ti_{50}$ alloy powders after selected MD times.

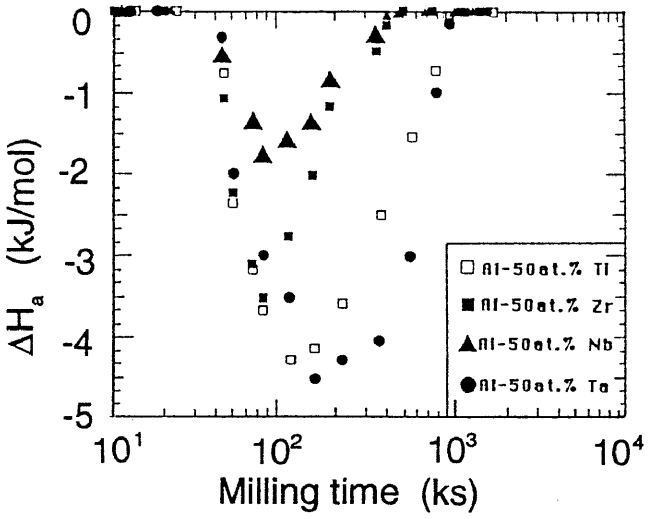

Fig. 33 Effect of the MA times on the enthalpy change of amorphization, ΔH_a, for rod-milled $Al_{50}TM_{50}$ (TM; Ti, Zr, Nb and Ta) alloy powders.

and 154 kJ/mol for $Al_{50}Ti_{50}$, $Al_{50}Zr_{50}$, $Al_{50}Nb_{50}$ and $Al_{50}Ta_{50}$, respectively. We should emphasize that the value of E_a is independent of MA time and does not change remarkably with increasing milling time, as was described in the previous papers[25,71,72,73,82].

It is worth mentioning that in MD alloy powders the exothermic reaction peaks which are attributed to a solid-

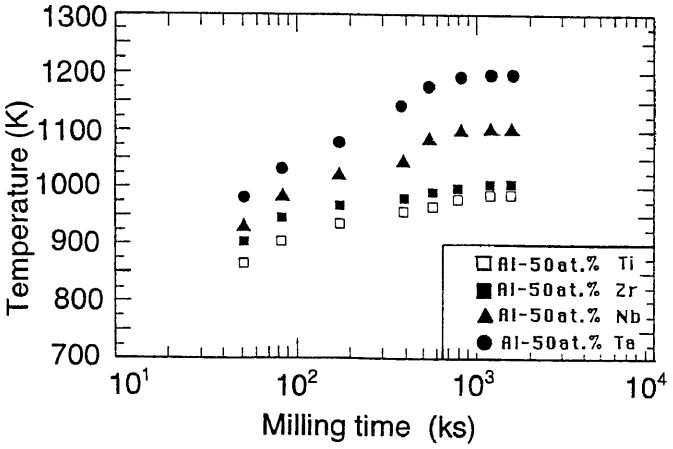

Fig. 34 Effect of the MA times on the crystallization temperature, T_x, for rod-milled $Al_{50}TM_{50}$ (TM; Ti, Zr, Nb and Ta) alloy powders.

state amorphizing reaction at the fresh surfaces of Al/TM boundaries, are absent, as shown in Fig.32. The DTA curves of MD AlTi alloy powders reveal single exothermic peak which develop during MD. After 1440 ks of MD time, a sharp exothermic peak is observed at about 890 K.

Figure 33 illustrates the change of ΔH_a for mechanically alloyed $Al_{50}Ta_{50}$ powders during the MA process. At the amorphization stage of milling, ΔH_a decreases sharply and approaches a minimum value. Then, ΔH_a tends to increase monotonically to be almost nil towards the end of the amorphization stage.

The crystallization characteristics of mechanically alloyed $Al_{50}Ta_{50}$ powders indexed by the T_x (temperature of the crystallization peak) is shown in Fig.34. T_x increases drastically with increasing the milling time at the amorphization stage of milling, indicating a continuous change of the composition of the amorphous phase. At the final stage of the MA time, T_x approaches a saturation, as shown in Fig.34.

Table I summarizes some of the measured thermodynamics properties of the end-product for rod-milled $Al_{50}TM_{50}$ alloys.

4. Summary

This is a systematic study of the mode of amorphization and crystallization for rod-milled and/or ball-milled $Al_{50}TM_{50}$ (TM; Ti, Zr, Nb and Ta) alloys. The present study allows the following interpretations:

(1) The mechanical alloying (MA) and/or mechanical disordering (MD) processes have been employed for producing new amorphous alloys such as Al-Ta binary system that is extremely difficult or impossible to produce by conventional melting and casting techniques. MA process leads to the formation of an extraordinarily high thermal stable Al_xTa_{1-x} amorphous alloy powders in the range of $0.25< x <0.90$.

(2) The crystallization temperature ,T_x, increases monotonically with increasing Ta content to reach to a high value, as a high as of 1216 K.

(3) The amorphous alloy powders produced by the BM technique are suffering from the high iron contamination content which reach to more than 10 at.% in Ta rich side.

Table 1
Some of the measured thermodynamic properties of the end-products for rod-milled Al-50 at % TM alloys.

TM	E_a (kJ/mol)	T_x (K)	T_x/T_m	ΔH_x (kJ/mol)
Ti	-168	993	0.55	-63
Zr	-156	1000	0.56	-68
Nb	-179	1105	0.50	-13
Ta	-154	1200	0.54	-45

(4) The rod-milling (RM) technique has been investigated for the first time to produce amorphous alloy powders with a low iron contamination content, less than 1 at.%.

(5) The MA process for producing amorphous alloy powders of $Al_{50}TM_{50}$ can be classified into three stages, that is to say, agglomeration, amorphization and homogenization stages. The agglomeration stage (0 to 43 ks) may be refereed to the first milling stage of the MA process. At this stage, the powders are agglomerated to form larger particles, as large as 1000 mm. The powder particles have layered structure morphology and contain many coarse layers of Al and TM elements.

At amorphization stage (43 to 360 ks) a dramatical disintegration of the powder particles occurs and the particles are reduced sharply in size. All of the particles contain many narrow layers in a good arrangement as a result of the shear force which is generated by the rods. Heating the alloy powders to about 700 K leads to the formation of an amorphous phase by a thermally-assisted amorphization (TASSA) which is conducted between the elemental layers of Al and TM layers. As the the composite particles contain many layers, the enthalpy change of amorphization, ΔH_a decreases sharply as a consequence of the solid-state diffusion between these layers. ΔH_a increases dramatically with decreasing the number of the layers in the particles. When the powder particles have not any layers, heating them in the DTA does not lead to the formation of any amorphous phases and ΔH_a becomes nil. During this stage, both of the crystallization temperature, T_x and the enthalpy change of crystallization, $-\Delta H_a$ increase monotonically. The amorphization stage is a unique in that, an amorphous alloy can be obtained just by heating the layered-particles to about 700 K without further milling. The activation energy of amorphization has been calculated for $Al_{50}TM_{50}$ to be in the range of 170 kJ/mol.

The homogenization stage (360 to 1440 ks) can be defined as the last stage of milling in which the solid-state amorphizing reaction takes place homogeneously to get a uniform amorphous phase. The layered-structure morphology disappear and the shape of the powder particles changes to be almost spherical with size less than 1 μm in diameter.

Finally, it has been the goal of the present study to produce new metallic amorphous alloys and adding a new novel technique for SSAR process.

Acknowledgments

The authors are grateful to the Ministry of Education, Science and Culture of Japan for financial support of a grant-in-Aid for Development Scientific Research B (03555139) and Grant-in-Aid for Co-operative Research (03302053)

One of the authors (M. Sherif) is indebted to Prof. A. Inoue , Prof. R. Watanabe and Prof. K. Sumiyama for fruitful discussions motivating this investigation and continuous supporting the present study.

The authors wish to express their deep thanks to Dr. Y. Minonishi and Dr. S. Yano for useful comments and suggestions.

We would like to acknowledge Mr. E. Aoyagi and Ms. W. Morita for suggested TEM observations. Many thanks to Mr. Y. Murakami for his kind assistance during the SEM observations.

The authors are indebted to Mr. Y. Danzaki and Dr. K. Takada for the suggested chemical analysis explanations.

We would like also to thank the NEC company for supporting this study and providing us with high-grade Ta and Nb powders.

References

(1) R.B. Schwarz and W.L. Johnson, Phys. Rev. Lett., 51 (1983) 415.
(2) Y.T. Cheng, W.L. Johnson and M.A. Nicolet, Appl. Phys. Lett., 47 (1985) 800.
(3) H. Schroder, K. Samwer and U. Koster, Phys. Rev. Lett., 54 (1985) 197.
(4) A.Y. Yermakov, Y.Y. Yurchikov and V.A. Barinov, Phys. Met. Metall., 52 (1981) 50.
(5) R.L. White, Ph.D Thesis, Stanford University, 1977.
(6) C.C. Koch, O.B. Cavin, C.G. McKamey and J.O. Scarbrough, Appl. Phys. Lett., 43 (1983) 1017.
(7) S.R. Elliott, Physics of Amorphous Materials (Longman Scientific & Technical, (1990) p. 25.
(8) J.S. Benjamin, Met. Trans., 1A (1970) 2943.
(9) I.G. Wright and A. Wilox, Met. Trans., 5A (1974) 957.
(10) J.S. Benjamin and T.E. Volin, Met. Trans., 5A (1974) 1929.
(11) J.S. Benjamin, Sci. Am., 40 (1976) 234.
(12) G.H. Gessinger, Met. Trans., 1A (1976) 1203.
(13) J.S. Benjamin and M.J. Bomford, Met. Trans., 8A (1977)1301.
(14) P.S. Gilman and W.D. Nix, Met. Trans., 12A (1981) 813.
(15) J. S. Benjamin and R.D. Schelleng, Met.Trans.,12A (1981) 1827.
(16) K. Suzuki, J. Non-Cryst. Solids, 117/118 (1990) 1.
(17) K. Suzuki, J. Non-Cryst. Solids, 112 (1989) 23.
(18) W.L. Johnson, Prog. in Mater. Sci. , 30 (1986) 81.
(19) E. Hellstern and L. Schultz, Appl. Phys. Lett., 48 (1986) 124.
(20) R.B. Schwarz, R.R. Petrich and C.K. Saw, J. Non-Cryst. Solids, 76 (1985) 281.
(21) M. Atzmon, K. Unruh and W.L. Johnson, J. Appl. Phys., 58 (1985) 3865.
(22) M. Sherif El-Eskandarany, F. Itoh, K. Aoki and K. Suzuki, J. Non-Cryst. Solids, 117/118 (1990) 729.
(23) E. Hellstern and L. Schultz, Appl. Phys. Lett., 53 (1986) 1399.
(24) M. Sherif El-Eskandarany, K. Aoki and K. Suzuki, Scripta Metall., 25 (1991) 1695.
(25) M. Sherif El-Eskandarany, K. Aoki and K. Suzuki, J. Appl. Phys., 71 (1992) 2924.
(26) T. Fukunaga, K. Nakamura, K. Suzuki and U. Mizutani, J. Non-Cryst. Solids, 117/118 (1990) 700.
(27) E. Gaffet and M. Harmelin, J. Less-Common Met., 157 (1990) 201.
(28) M. Sherif El-Eskandarany, K. Sumiyama, K. Aoki and K. Suzuki, J. Mater. Res., 7 (1992) 888.
(29) M. Sherif El-Eskandarany, K. Sumiyama, K. Aoki and K. Suzuki, Mater. Sci. Forum, 88-90 (1992) 801.
(30) M. Sherif El-Eskandarany, K. Aoki and K. Suzuki, Appl. Phys. Lett., 60 (1992) 1562.
(31) R. Schwarz and C.C. Koch, Appl. Phys. Lett., 49 (1986) 146.
(32) A.W. Weeber, K van der Meer, H. Bakker, F.R de Boer, B.J. Thijsse and J.F. Jongste, J. Phys.F: Met. Phys., 16 (1986).
(33) E. Hellstern and L. Schultz, Appl. Phys. Lett., 49 (1986) 1163.
(34) B.P. Dolgin, M.A. Vanek, T. McGory and D.J. Ham, J. Non-Cryst. Solids, 87 (1986) 281.
(35) P.Y. Lee and C. Koch, J. Non-Cryst. Solids, 94 (1987) 88.
(36) F. Itoh, T. Sekiuchi, M. Sakurai, T. Fukunaga and K. Suzuki, Trans. JIM, 29 (1988) 127.
(37) R.B. Schwarz and R.R. Petrich, J. Less-Common Met., 140 (1988) 171.
(38) P.I. Loeff and H. Bakker, Scripta Metall., 22 (1988) 401.
(39) J. Eckert and L. Schultz, J. Less-Common Met., 145 (1988) 283.
(40) E. Gaffet, N. Merk, G. Martin and J. Bigot, J. Less-Common Met., 145 (1988) 251.
(41) P.Y. Lee, J. Jang and C. Koch, J. Less-Common Met., 140 (1988) 73.
(42) P.I. Loeff, F.H.M. Spit and H. Bakker, J. Less-Common Met., 145 (1988) 271.
(43) H. Kimura, F. Takada and W.N. Myung, Mater. Sci. Eng., 97 (1988) 125.
(44) E. Ivanov, T. Grigorieva, G. Golubkova, V. Boldyrev, A.B. Fasman, S.D. Mikhailenko and O.T. Kalinina, Mater. Lett., 7 (1988) 51.
(45) A. Calka and A.P. Radlinski, Mater. Sci. Eng., 118 (1988) 131.
(46) G. Cocco, S. Enzo, N. Barrett and J. Roberts, J. Less-Common Met., 154 (1988) 177.
(47) K. Matsuki, A. Inoue, H.M. Kimura and T. Masumoto, Mater. Sci. Eng., 97 (1988) 47.
(48) T. Nasu, K. Nagaoka, S. Takahashi, T. Fukunaga and K. Suzuki, Trans. JIM, 30 (1989) 146.
(49) K.F. Kobayashi, N. Tachibana and P.H. Shingu, J. Mater. Sci., 24 (1989) 2437.
(50) K.F. Kobayashi, N. Tachibana and P.H. Shingu, J. Mater. Sci., 25 (1990) 801.
(51) J.S. Jang and C. Koch, J. Mater. Res., 5 (1990) 498
(52) H.J. Fecht, G. Han, Z. Fu and W.L. Johnson, J. Appl. Phys., 67 (1990) 1744.
(53) B. Huang, N. Tokizane, K.N. Ishihara, P.H. Shingu

and S. Nasu, J. Non-Cryst. Solids, 117/118 (1990) 688.
(54) C.H. Lee, M. Mori and U. Mizutani, J. Non-Cryst. Solids, 117/118 (1990) 733.
(55) J. Eckert, L. Schultz and K. Urban, J. Mater. Sci., 26 (1991) 441.
(56) A. Corrias, G. Ennas, G. Marongiu and G. Paschina, J. Mater. Sci., 26 (1991) 5081.
(57) A. Calka, A.P. Radlinski and R. Shanks, Mater. Sci. Eng. , 133 (1991) 555.
(58) T. Ogasawara, A. Inoue and T. Masumoto, Mater. Sci. Eng., 143 (1991) 1338.
(59) E. Gaffet, C. Louison, M. Harmelin and F. Faudot, Mater. Sci. Eng., 134 (1991) 1380.
(60) T. Nasu, C.C. Koch, K. Nagaoka, N. Itoh, M. Sakurai and K. Suzuki, Mater. Sci. Eng., 134 (1991) 1385.
(61) Y.S. Cho and C. Koch, Mater. Sci. Eng., 141 (1991) 139.
(62) Y.H. Park, H. Hashimoto and R. Watanabe, Mater. Sci. Forum, 88-90 (1992) 155.
(63) J. H. Ahn, H.S. Chung, R. Watanabe and Y.H. Park, Mater. Sci. Forum, 88-90 (1992) 347.
(64) E. Ivanov, Mater. Sci. Forum, 88-90 (1992) 475.
(65) A. Inoue, K. Matsuki and T. Masumoto, Mater. Sci. Forum, 88-90 (1992) 305.
(66) Y. Homma, T. Fukunaga and K. Suzuki, Mater. Sci. Forum, 88-90 (1992) 339.
(67) M. Sherif El-Eskandarany, K. Aoki and K. Suzuki, J. Less- Common Met., 167 (1990) 113.
(68) M. Sherif El-Eskandarany, K. Aoki and K. Suzuki, J. Jpn. Soc. of Powder and Powder Metall. (JSPM), 38 (1991) 934.
(69) M. Sherif El-Eskandarany, K. Aoki and K. Suzuki, Forum, 88-90 (1992) 81.
(70) M. Sherif El-Eskandarany, K. Aoki and K. Suzuki, J. Non-Cryst. Solids, 150 (1992) 472.
(71) M. Sherif El-Eskandarany, K. Aoki and K. Suzuki, J. Alloys Comp., 186 (1992) 15.
(72) M. Sherif El-Eskandarany, K. Aoki and K. Suzuki, Met. Trans., 23A (1992) 1231.
(73) M. Sherif El-Eskandarany, K. Aoki and K. Suzuki, J. Appl. Phys., 72 (1992) 2665.
(74) A.W. Weeber and H. Bakker, Physica B , 153 (1988) 93.
(75) K. Suzuki, J. Phys: F, 3 (1991) 39.
(76) C.C. Koch, Mechanical Milling and Alloying (Processing of Metals and Alloys, ed R.W Cahn. VCLT 1991) p.193.
(77) Company of NEC (private communication), 1989.
(78) P.R. Subramanian, D.B. Miracle and S. Mazdiyasni, Met. Trans., 21A (1990) 539.
(79) M. Sherif El-Eskandarany, K. Aoki, H. Itoh and K. Suzuki, J. Less-Common Met., 169 (1991) 235.
(80) A.R. Miedema, J. Less-Common Metals, 32 (1973) 117.
(81) A.R. Miedema, J. Less-Common Metals, 46 (1976) 67.
(82) M. Sherif El-Eskandarany, Ph.D Thesis, Tohoku University, 1992.
(83) M. Sherif El-Eskandarany, K. Aoki and K. Suzuki, J. Alloys Comp., 177 (1991) 229.